Phosphorothioate Substitution Can Substantially Alter RNA Conformation†

Jeff S. Smith‡ and Edward P. Nikonowicz*

Department of Biochemistry and Cell Biology, Rice University, Houston, Texas 77005

Received November 24, 1999; Revised Manuscript Received March 6, 2000

ABSTRACT: Phosphorothioate substitution−interference experiments, routinely used to stereospecifically identify phosphoryl oxygen sites that participate in RNA−ligand binding and RNA-directed catalysis, rest in their interpretation on the untested assumption that substitution does not alter the conformation of the modified molecule from its biologically active state. Using NMR spectroscopy, we have tested this assumption by determining the structural effect of stereospecific phosphorothioate substitution at five positions in an RNA hairpin containing the binding site for bacteriophage MS2 capsid protein. At most sites, substitution has little or no effect, causing minor perturbations in the phosphate backbone and increasing the stacking among nucleotides in the hairpin loop. At one site, however, phosphorothioate substitution causes an unpaired adenine necessary for formation of the capsid protein−RNA complex to loop out of the RNA helix into the major groove. These results indicate that phosphorothioate substitution can substantially alter the conformation of RNA at positions of irregular secondary structure, complicating the use of substitution−interference experiments to study RNA structure and function.

The chemical modification of biological molecules at specific functional groups is a useful and widespread technique for studying macromolecular structure and function (*1*). Phosphorothioate modification of RNA molecules, in which one of the two phosphoryl oxygen atoms is replaced with a sulfur atom, can be used to identify phosphate sites important for RNA−ligand binding or RNA-directed catalysis. Although the van der Waals radii, bond lengths, and electrostatic charges of sulfur and oxygen atoms are very similar, the different charge distribution and polarizability of phosphorothioates can alter the strength of ionic and hydrogen bonds and thus alter RNA−ligand affinities. Alternatively, functionally important sites can be identified by the inability of iodine to cleave phosphorothioates protected by bound ligands. Phosphorothioate substitution−interference experiments have identified specific RNA phosphoryl oxygen sites involved in the coordination of catalytic and structural metal ions (*2*−*6*) and in the formation of direct contacts with specific proteins (*7, 8*).

Central to the interpretation of chemical modification−interference experiments is the assumption that modification does not significantly alter the conformation of the modified molecule from its biologically active state. To date, however, this assumption has been directly tested for phosphorothioate substitution only in helical DNA molecules, where substitution has at most minor effects. Crystal structures of unmodified and phosphorothioate-modified DNA duplexes are very similar (*9*). Uniform or single-site substitutions in the DNA strand of DNA:RNA hybrid duplexes have little effect on overall duplex structure but cause adjacent deoxyribose sugars to populate to a greater extent the C3′-*endo* conformation (*10, 11*). Similar patterns are seen for both the R_P and S_P stereoisomers (Figure 1), suggesting that the chirality of the phosphorothioate makes little difference (*11*).

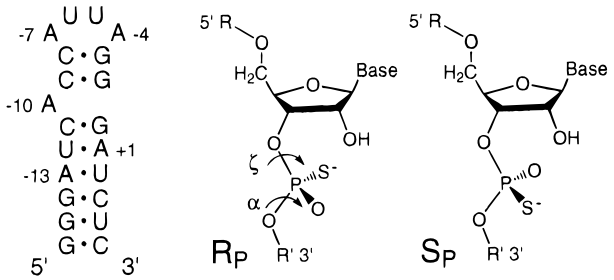

FIGURE 1: (A, left) Sequence of the RNA hairpin used in this study, containing the binding site for phage MS2 capsid protein. A_{+1} indicates the first nucleotide of the translation start codon of the MS2 replicase gene. Phosphorothioates in the sRNA hairpin are located 5′ to every adenine residue. (B, right) R_P and S_P phosphorothioate stereoisomers. Only the S_P stereoisomer is a substrate for T7 RNA polymerase, which incorporates 5′-α-thio-NTPs with inversion of configuration. All phosphorothioates in the sRNA hairpin are of the R_P stereoisomer.

Despite these studies, little is known about the effects of phosphorothioate substitution on the conformation of RNA molecules, which more often contain functionally important regions of single-stranded and irregular secondary structure that might be more easily disrupted by chemical modification. To assess the degree to which phosphorothioate substitution alters the conformation of RNA, we have determined the solution structure of an RNA hairpin containing the binding site for bacteriophage MS2 capsid protein and the structure of the same hairpin in which the phosphates 5′ to all five adenine nucleotides have been replaced by R_P phosphorothioates (Figure 1). Two of these substitutions are in regions

† This work was supported by National Institutes of Health Grant GM52115 and Robert A. Welch Foundation Grant C-1277 to E.P.N.

* Address correspondence to this author. E-mail: edn@bioc.rice.edu. Telephone: (713) 348-4912. Fax: (713) 348-5154.

‡ Present address: Department of Biology, Emory University, Atlanta, GA 30322.

10.1021/bi992712b CCC: $19.00
Published on Web 04/19/2000

of helical duplex, two are in the hairpin tetraloop, and one is adjacent to an unpaired adenine residue between the upper and lower helices.

MATERIALS AND METHODS

All enzymes were purchased (Sigma) except for T7 RNA polymerase, which was prepared as described (*12*). Deoxyribonuclease I type II, pyruvate kinase, adenylate kinase, and nucleotide monophosphate kinase were obtained as powders, dissolved in solutions of 15% glycerol, 1 mM dithiothreitol, and 10 mM Tris-HCl, pH 7.4, and then stored at −20 °C. Guanylate kinase and nuclease P_1 were obtained as solutions and stored at −20 °C. Unlabeled 5′-nucleoside triphosphates (5′-NTPs) and 5′-α-thioadenosine monophosphate (Sigma), phosphoenolpyruvate (potassium salt) (Bachem), and 99% [^{15}N]ammonium sulfate and 99% [^{13}C]glucose (Cambridge Isotope Labs) were obtained as powders.

Preparation of RNA Samples. Phosphorothioate-modified and unmodified RNA molecules (Figure 1) were prepared by in vitro transcription using T7 RNA polymerase and synthetic DNA templates (*13*). Isotopically enriched 5′-NMPs were prepared as described (*14*), sequentially eluted from an anion exchange column using a stepped gradient of formic acid (*15*), and converted to 5′-NTPs. 5′-α-Thio-AMP was enzymatically converted to 5′-α-thio-ATP as described (*16*). Unlabeled all-phosphate-containing RNA hairpin (oRNA)[1] was prepared from 20 mL transcription reactions using 4 mM 5′-NTPs, and phosphorothioate-containing RNA hairpin (sRNA) was prepared using 4 mM 5′-{GTP, CTP, and UTP} and 4 mM 5′-α-thio-ATP. Isotopically labeled RNA was prepared similarly except that the transcription volumes were 16 mL and the concentration of NTPs was 3 mM. RNA molecules were purified by passage through 20% (w/v) preparative polyacrylamide gels, electroeluted (Schleicher & Schuell), and precipitated with ethanol. The purified oligonucleotides were dissolved in 1.0 M NaCl, 20 mM potassium phosphate, pH 6.8, and 2.0 mM EDTA and dialyzed extensively against 10 mM NaCl, 10 mM potassium phosphate, pH 6.8, and 0.05 mM EDTA using a Centricon-3 concentrator (Amicon Inc.). Samples were diluted with buffer to a volume of 250 μL, lyophilized to powders, and resuspended in 250 μL of either 99.96% ^2H_2O or 90% ^1H_2O/10%^2H_2O. Samples contained 110−130 A_{260} OD units in 250 μL (≈2.5−3.0 mM).

NMR Spectroscopy and Structure Calculations. All NMR spectra were acquired at 500 MHz (Bruker, AMX) with a ^{1}H-{X} reverse detection probe, except for ^{1}H-{^{13}C-^{31}P} triple resonance experiments which were acquired at 600 MHz (Varian, Unity Plus). Broadband decoupling of ^{13}C and ^{15}N resonances was achieved using GARP with $\gamma B_2 = 3125$ Hz for carbon and $\gamma B_2 = 1570$ Hz for nitrogen. Spectra were collected in 90% ^1H_2O at 12 °C using binomial read pulses with maximum excitation at 12.5 and 8.0 ppm. Experiments in ^2H_2O were acquired at 27 °C with presaturation or spin-lock pulses to suppress the residual HDO peak. Quadrature detection was achieved using the States-TPPI method, and acquisition was delayed by a half-dwell in all indirectly detected dimensions. Acquisition times for most two-dimensional (2D) experiments were $\omega_1 = 46-50$ ms and $\omega_2 = 168-228$ ms and for most three-dimensional (3D) experiments were $\omega_{^1H} = 22-28$ ms, $\omega_{^{13}C/^{15}N} = 20-36$ ms, and $\omega_{^1H} = 168-228$ ms. Typically, the data points were extended by 33% using linear prediction for the indirectly detected dimensions, and the data were apodized using 1 Hz line broadening and 65° shifted sinebell functions. ^{1}H spectra were referenced to the internal HDO resonance at 4.76 ppm at 25 °C. The ^{13}C, ^{15}N, and ^{31}P spectra were referenced to external standards of TSP, NH_4OH, and TMP, respectively, which resonate at 0.00 ppm. All spectra were processed and analyzed with Felix 97.0 (Molecular Simulations, Inc.).

2D ^{13}C-^{1}H HMQC and HSQC spectra were collected to identify ^{13}C-^{1}H chemical shift correlations. 3D HCCH-COSY and HCCH-TOCSY (24 ms DIPSI-3 spin-lock) experiments optimized for polarization transfer through the ribose carbons and a 2D ^{13}C-^{1}H HCCH-TOCSY (52 ms DIPSI-3 spin-lock) optimized for polarization transfer through the adenine bases (oRNA only) were collected in ^2H_2O to identify ribose spin systems and H8−H2 correlations, respectively (*17, 18*). To identify intraresidue base−sugar correlations, a 2D ^{15}N-^{1}H HSQC experiment was acquired in ^2H_2O and optimized for two- and three-bond correlations as reported (*19*), except that the ^{15}N-^{1}H anti-phase magnetization was refocused after the t_1 evolution period to achieve cross-peaks that were *in-phase* in ω_1 and ω_2 and to permit application of broadband ^{15}N decoupling during the t_2 acquisition period.

2D NOESY and 3D ^{13}C-edited NOESY experiments were collected in ^2H_2O at $\tau_m = 80$, 90, 180, 360, and 400 ms to obtain distance constraints for the nonexchangeable resonances. 2D ^{13}C-^{1}H half-filtered NOESY experiments were collected at $\tau_m = 180$ and 400 ms to aid assignment of adenine ^{1}H resonances and to obtain internucleotide distance constraints for the sRNA hairpin. For the exchangeable protons, 2D ^{15}N-^{1}H HSQC spectra were collected in 90% ^1H_2O to identify ^{15}N-^{1}H chemical shift correlations, and 2D NOESY and 3D ^{15}N-edited NOESY experiments were collected at $\tau_m = 220$, 300, and 360 ms to obtain distance constraints. 2D ^{31}P-^{1}H hetero-TOCSY-NOESY experiments were acquired using unlabeled RNA samples to obtain ^{31}P resonance assignments.

Backbone dihedral angle constraints were derived from spectra collected to measure ^{1}H-^{1}H, ^{31}P-^{1}H, and ^{13}C-^{31}P coupling constants. Using unlabeled RNA samples, ^{31}P-decoupled DQF-COSY experiments and ^{31}P-^{1}H HetCor experiments with supression of ^{1}H-^{1}H passive coupling (*20*) were collected in ^2H_2O with acquisition times of $\omega_1 = 119$ ms and $\omega_2 = 408$ ms and $\omega_1 = 64$ ms and $\omega_2 = 408$ ms, respectively. Three-bond ^{31}P-^{13}C coupling constants were derived from 2D ^{13}C-^{1}H HSQC spin−echo difference experiments with and without ^{31}P decoupling in t_1 (*21*). Two separate spin−echo experiments were acquired for the sRNA hairpin using ^{31}P carrier positions centered at −3.5 and 52.0 ppm.

Interproton Distance Constraints. Semiquantitative distance constraints between nonexchangeable protons were estimated from cross-peak intensities in 2D NOESY and 3D ^{13}C-edited NOESY spectra at mixing times of 80, 90, 180,

[1] Abbreviations: NOE, nuclear Overhauser enhancement; NOESY, NOE spectroscopy; DQF-COSY, double quantum filtered correlated spectroscopy; 2D, two-dimensional; 3D, three-dimensional; HMQC, heteronuclear multiple quantum coherence; MD, molecular dynamics; NH, imino; NH_2, amino; oRNA, all-phosphate RNA; sRNA, phosphorothioate-modified RNA.

360, and 400 ms. Using the covalently fixed pyrimidine H5−H6 distance (≈2.4 Å) and the conformationally restricted sugar H1′−H2′ distance (2.8−3.0 Å) as references, peak intensities were classified as strong, medium, weak, or very weak and their corresponding proton pairs given upper bound distance constraints of 3.0, 4.0, 5.0, or 6.0 Å, respectively. Cross-peaks observed only at mixing times greater than 300 ms were classified as extremely weak and given 7.0 Å upper bound distance constraints to account for the possibility of spin diffusion. To improve convergence of the calculations, all distance constraints were given lower bounds of 0.0 Å, except for three extremely weak distances in the sRNA molecule that were consistently too close in calculated structures to be consistent with the observed NMR data. These constraints were given lower bounds of 3.0 Å. Distance constraints involving exchangeable protons were estimated from ^{1}H-^{1}H and 2D ^{15}N-^{1}H 220, 300, and 360 ms mixing time NOESY spectra and were classified as either weak, very weak, or extremely weak, except for the intrabase pair distances A·U H2−NH, G·C NH−NH_2, and G·U NH−NH, which were classified as strong constraints. Intraresidue sugar-to-sugar constraints were included in the calculations only for distances involving H5′/H5″ atoms.

Hydrogen Bonding Constraints. Watson−Crick base pairs were identified using two criteria: the observation of a significantly downfield shifted NH or NH_2 proton resonance and the observation of strong G·C NH−NH_2 or A·U H2−NH NOEs. The wobble G·U pair was identified by observation of a strong NOE between guanine and uridine NH resonances. Hydrogen bonds were introduced as distance restraints of 3.1 ± 0.5 Å between donor and acceptor heavy atoms and 2.15 ± 0.35 Å between acceptor and hydrogen atoms. Individual hydrogen bonds were also constrained to be roughly linear (180 ± 40°). Constraints identified in this way were included in the calculations for base pairs G_{-16}·C_{+5}, G_{-15}·U_{+4}, G_{-14}·C_{+3}, A_{-13}·U_{+2}, U_{-12}·A_{+1}, C_{-9}·G_{-2}, and C_{-8}·G_{-3}.

Dihedral Angle Constraints. Constraints on the ribose ring and backbone dihedral angles were derived from semiquantitative measurements of $^{3}J_{H-H}$, $^{3}J_{H-P}$, and $^{3}J_{C-P}$ couplings (*20*, *21*). Sugar pucker conformations were determined from $^{3}J_{H1'-H2'}$ couplings in ^{31}P-decoupled 2D DQF-COSY spectra. Residues with couplings >7 Hz were constrained to the C2′-*endo* conformation through three of the torsion angles in the ribose sugar ring (*22*). Independent confirmation of sugar pucker conformation was provided by the observation of weak (<5 Hz) $^{3}J_{H3'-H4'}$ couplings, C3′ resonances shifted downfield to 76−80 ppm from the main cluster at 70−72 ppm, and C4′ resonances shifted downfield to 85−86 ppm from the main cluster at 82−84 ppm (*23*). Residues with weak (<5 Hz) $^{3}J_{H1'-H2'}$ couplings and large (>5 Hz) $^{3}J_{H3'-H4'}$ couplings were constrained to the C3′-*endo* conformation. Residues with intermediate $^{3}J_{H1'-H2'}$ couplings were left unconstrained to reflect the possibility of conformational averaging.

Dihedral angle constraints for the γ torsion angles were derived from $^{3}J_{H4'-H5'}$ and $^{3}J_{H4'-H5''}$ couplings in the DQF-COSY spectrum and intraresidue H4′−H5′ and H4′−H5″ cross-peak intensities in a 80 ms mixing time 3D NOESY-ctHSQC spectrum. For residues in which H4′−H5′ and H4′−H5″ peaks in the DQF-COSY spectra were clearly absent, representing couplings <5 Hz, γ was constrained to the gauche^{+} conformation (60 ± 20°) (*22*, *24*). For residues with only weak or unobservable $^{3}J_{H4'-H5'}$ or $^{3}J_{H4'-H5''}$ couplings or with unequal H4′−H5′ and H4′−H5″ NOE intensities, γ was left unconstrained to reflect the possibility of conformational averaging.

Dihedral angle restraints for the β and ϵ torsion angles were derived from $^{3}J_{P-H5'}$, $^{3}J_{P-H5''}$, and $^{3}J_{P-H3'}$ couplings measured in 2D ^{31}P-^{1}H HetCor spectra and $^{3}J_{P-C2'}$ couplings measured in 2D ctHSQC spectra. β was constrained to the trans conformation (180 ± 20°) for residues in which P−H5′ and P−H5″ peaks in the HetCor spectra were clearly absent, representing couplings <5 Hz (*22*, *24*). For residues in which P−H5′ and P−H5″ peaks could be observed, β was left unconstrained to reflect the lack of stereospecific assignments and the possibility of conformational averaging. ϵ was constrained to the trans conformation (−145 ± 20°) for residues with $^{3}J_{P-H3'}$ > 5 Hz and $^{3}J_{P-C2'}$ < 5 Hz and to the gauche^{-} conformation (−100 ± 25°) for residues with $^{3}J_{P-H3'}$ > 5 Hz and $^{3}J_{P-C2'}$ > 5 Hz (*22*, *24*). Residues with $^{3}J_{P-H3'}$ > 5 Hz but for which $^{3}J_{P-C2'}$ could not be measured, or for which $^{3}J_{P-C2'}$ and $^{3}J_{P-C4'}$ couplings were inconsistent with a single conformation, were loosely constrained to include both conformations (−120 ± 45°). No dihedral angle constraints were used for the backbone angles α and ζ or for the glycosidic angle χ.

Structure Calculations. All calculations were carried out on Silicon Graphics Indy workstations using X-PLOR 3.851 (*25*). The dihedral angles of a model structure (generated using Insight II, Molecular Simulations, Inc.) were randomized to generate 30 starting structures which were used in a simulated annealing/restrained molecular dynamics (rMD) routine (*22*). The force field was modified to include phosphorothioate functional groups (*26*). The calculation protocol was divided into two stages: global fold and refinement. The global fold step consisted of 1000 cycles of unconstrained conjugate gradient energy minimization, 7 ps of rMD at 1000 K using only hydrogen bond and NOE constraints, 22 ps of rMD at 1000 K during which repulsive van der Waals forces were introduced, 4 ps of rMD at 1000 K during which the β, γ, ϵ, and sugar ring dihedral constraints were slowly introduced, 28 ps of rMD while cooling to 300 K, and 1000 cycles of constrained minimization. The structures were then refined using all constraints and attractive van der Waals potentials for 1000 cycles of constrained minimization, 5 ps of rMD at 300 K, and another 1000 cycles of final minimization. To determine the consistency of the NMR data with different possible ribose ring puckers of the bulged adenine nucleotide, two additional sets of calculations were performed for each oligonucleotide: one with the A_{-10} sugar constrained to the C3′-*endo* conformation and one with the A_{-10} sugar constrained to the C2′-*endo* conformation. All calculated structures were viewed using MidasPlus (UCSF) and Insight II. Coordinates and experimental constraints for the phosphate and the phosphorothioate-modified RNA molecules have been deposited at the PDB as 1D0U and 1D0T, respectively.

Thermal Stability. UV melting studies were performed using 2.2 μM RNA hairpin dissolved in NMR buffer (10 mM NaCl, 10 mM potassium phosphate, pH 6.8, and 0.05 mM EDTA). A_{260} absorbance spectra from 40 to 90 °C were acquired (1.0 °C per minute) on a Pharmacia Ultrospec 2000 UV−Visible spectrophotometer equipped with a Peltier

melting apparatus. The melting curves were acquired in triplicate and were fit to a two-state model. Base proton chemical shift transition midpoints (T_{cs}) were measured using 2D ^{13}C-^{1}H ct-HSQC spectra collected from 25 to 70 °C at 5 °C intervals, except from 50 to 65 °C, where intervals were 2.5 °C. The temperature dependencies of the adenine H2 resonances of the sRNA hairpin were determined using one-dimensional ^{1}H spectra.

RESULTS

Resonance Assignments and Chemical Shifts. The ^{1}H, ^{13}C, ^{15}N, and ^{31}P resonances of the unmodified (oRNA) and phosphorothioate-modified (sRNA) hairpins were assigned using standard heteronuclear methods (*27*, *28*). Resonances of the sRNA adenine nucleotides, which are not isotopically enriched, were assigned using ^{13}C-^{1}H filtered experiments (*29*). The chemical shifts of most resonances differ only slightly between the two molecules. Those resonances with substantial differences are often adjacent to phosphorothioate positions, probably reflecting the different chemical and electrostatic properties of the sulfur atom (*30*, *31*). For example, the H3′ resonances of G_{-14}, C_{-11}, C_{-8}, U_{-5}, and G_{-1} are shifted 0.15−0.35 ppm downfield, and the C3′ resonances of G_{-14} and G_{-1} are shifted ∼1.0 ppm downfield. The H8 resonances of A_{-4} and A_{-7} and the H4′ resonance of U_{-5} are shifted ∼0.25 ppm downfield, while the H4′ resonance of U_{-6} is shifted ∼0.3 ppm upfield. Some chemical shift differences, however, are at sites further removed from phosphorothioate positions and may reflect structural differences between the two molecules. In the sRNA molecule, for example, the most upfield H5′/H5″ resonances of residues C_{-9} and U_{-5} are shifted 0.2−0.3 ppm downfield, the C5′ resonance of C_{-9} is shifted ∼1.2 ppm downfield, and the G_{-1} NH resonance is shifted ∼0.1 ppm downfield. In addition, the G_{-2} NH resonance of the oRNA hairpin is broadened, probably due to exchange with solvent, while the corresponding resonance of the sRNA hairpin is not broadened (Figure 2). The differences in the G_{-2} and G_{-1} NH resonances suggest that the upper and lower helices may stack differently in the two molecules.

The ^{31}P resonances of phosphates in both molecules are dispersed between −3.4 and −4.6 ppm, while those of phosphorothioates resonate between 53.0 and 56.0 ppm (Figure 3). In the oRNA hairpin, the most downfield ^{31}P resonance is that of P_{-10}, and the resonances of P_{-13}, P_{-7}, P_{-4}, and P_{+1} are in the center of the main cluster at −4.0 ppm. In the sRNA hairpin, the relative positions of these resonances change as P_{-10} and P_{-4} are shifted >2 ppm upfield from P_{-13}, P_{-7}, and P_{+1} (Figure 3). The phosphate resonance of P_{-5} is shifted ≈0.4 ppm downfield in the spectrum of the sRNA molecule, suggesting long-range structural effects on the conformation of the loop sugar−phosphate backbone by phosphorothioates P_{-4} or P_{-7}. The other phosphate resonances differ <0.2 ppm between the two hairpins.

Structure Calculations. The structures of the oRNA and sRNA hairpins were calculated using a restrained molecular dynamics routine starting from 30 structures with completely random backbone dihedral angles. The calculations used a total of 448 distance constraints and 45 dihedral angle constraints for the oRNA hairpin and 313 distance constraints and 48 dihedral angle constraints for the sRNA hairpin; 11 oRNA and 13 sRNA converged structures were produced. Structures were classified as converged if they were consistent with the NMR data and maintained correct stereochemistry. All converged structures violated less than 5 NOE constraints by more than 0.1 Å and none by more than 0.3 Å, and when the structures were arranged in order of increasing overall energy, the converged structures formed a plateau with similarly low overall and constraint violation energies (*22*). The heavy atoms of all 21 nucleotides of the final converged structures superimpose on their average structures with average RMSDs of 1.49 and 1.73 Å, for the oRNA and sRNA hairpins, respectively. Additional structure calculation statistics are provided in Table 1.

Effect of Phosphorothioate Substitution on Conformation of the Bulge Region. NOESY spectra of the oRNA and sRNA hairpins are similar, but a few key differences indicate that

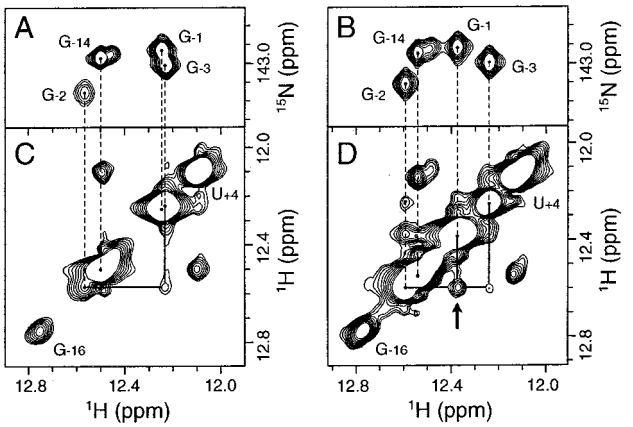

FIGURE 2: (A, B) Central NH regions of ^{15}N-^{1}H HMQC spectra of the (A) oRNA and (B) sRNA hairpins. The G_{-3} and G_{-1} NH resonances are nearly degenerate in the oRNA hairpin but are well separated in the sRNA hairpin. The G_{-2} NH resonance is broadened in the oRNA hairpin but not in the sRNA hairpin. (C, D) NH regions of ^{1}H-^{1}H NOESY spectra of the (C) oRNA and (D) sRNA hairpins. Solid lines trace sequential NH−NH NOE correlations through the bulge region. Dashed lines connect NH correlations of the NOESY and HMQC spectra. The arrow indicates an inter-base pair NOE between the G_{-2} and G_{-1} NH resonances that is present only in the spectrum of the sRNA hairpin. The G_{-15} NH of both hairpins resonate at 10.98 ppm and are not shown here.

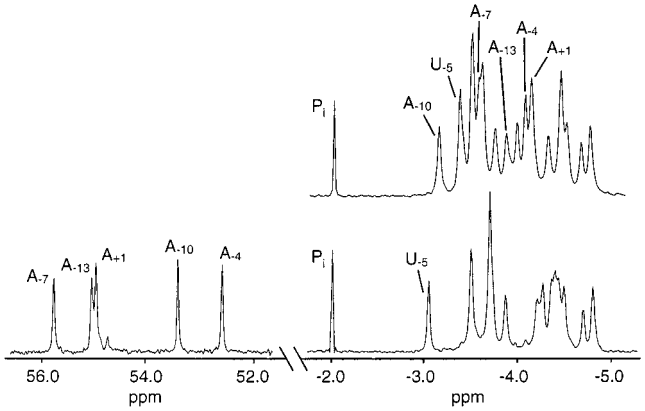

FIGURE 3: One-dimensional ^{31}P spectra of oRNA (top) and sRNA (bottom) hairpins. The ^{31}P resonances 5′ to each of the five adenine nucleosides are labeled. The phosphorothioate resonances are shifted ≈55 ppm downfield from the corresponding phosphates. The positions of the ^{31}P resonances 5′ to A_{-10} and A_{-4} relative to A_{+1}, A_{-7}, and A_{-13} differ between the oRNA and sRNA hairpins, indicating possible differences between the RNA hairpin backbone conformations.

Table 1: Summary of Experimental Distance and Dihedral Angle Constraints and Refinement Statistics[a]

parameter	oRNA	sRNA
NOE distance constraints[b]		
intraresidue	184	101
interresidue	264	212
mean number per residue	21.3	14.9
NOE constraints by category[c]		
strong (≤3.0 Å)	33	22
medium (≤4.0 Å)	73	23
weak (≤5.0 Å)	95	114
very weak (≤6.0 Å)	137	116
extremely weak (≤7.0 Å)	110	38[d]
base pair constraints[e]		
total	8	8
dihedral angle constraints[f]		
ribose ring	21	21
backbone	24	27
mean number per residue	2.1	2.3
violations		
average no. distance constraints >0.1 Å[g]	3.5 ± 1	0.5
RMSDs for distance constraints (Å)	0.015	0.010
average no. dihedral constraints >0.5° [h]	0.4 ± 0.1	0.2
RMSDs for dihedral constraints (deg)	0.056	0.055
RMSD from ideal geometry[i]		
bonds (Å)	0.004	0.004
angles (deg)	1.262	1.256

[a] Statistics are for oRNA and sRNA calculations with A_{-10} C3′-*endo* and C2′-*endo* constraints, respectively. [b] Only conformationally restrictive constraints are included. Intraresidue sugar-to-sugar constraints were included only for distances involving H5′/H5″ atoms. [c] Cross-peak intensities were obtained from 2D NOESY and 3D ^{13}C- and ^{15}N-edited NOESY spectra. Cross-peaks observed only at $\tau_m \geq$ 360 ms were classified as extremely weak. Cross-peaks involving exchangeable protons were classified as weak to extremely weak, except for intra-base pair A·U H2−NH, G·C NH−NH_2, and G·U NH−NH NOEs, which were classified as strong. [d] Three constraints were given lower bounds of 3.0 Å for atomic distances consistently too close to be consistent with NOE data. [e] Base pair constraints were applied for the eight base pairs in the upper and lower stems (Figure 1) based on the identification of NH−NH_2, NH−H2, and NH−NH NOE cross-peaks for G·C, U·A, and G·U base pairs, respectively. [f] Ribose sugar puckers were centered about either ideal C2′- or C3′-*endo* conformations or constrained to allow both conformations. Phosphate backbone torsion angles γ, β, and ϵ were restricted to t, g^-, or g^+ conformations ±25° (32). [g] A distance violation of 0.1 Å corresponds to a 5.0 kcal energy penalty. [h] A dihedral angle violation of 0.5° corresponds to a 0.003 kcal energy penalty. [i] Calculated for minimized average structures.

phosphorothioate substitution has a substantial effect on the conformation of the bulged A_{-10} nucleotide. For example, there is an inter-base pair NH−NH NOE between G_{-2} and G_{-1} in the NOESY spectrum of the sRNA hairpin that is absent from the corresponding spectrum of the oRNA hairpin (Figure 2). Similarly, interresidue $i - i+2$ sugar to base NOEs between C_{-11} and C_{-9} are present only in spectra of the sRNA hairpin, while sequential and cross-strand NOEs involving the A_{-10} H2 atom are present only in spectra of the oRNA hairpin. A summary of key NOEs is shown in Figure 4. Together, these NOE data indicate that the A_{-10} base is stacked between its flanking base pairs in the oRNA hairpin and unstacked or extrahelical in the sRNA hairpin.

Alterations in the sugar−phosphate backbone accompanying the change in A_{-10} conformation could not be detected due to insufficient NMR data. The ribose conformations of bulge region nucleotides (C_{-11}, A_{-10}, C_{-9}, G_{-2}, and G_{-1}), determined from $^3J_{H1'H2'}$ coupling constants and C1′ and C3′ chemical shifts, are similar for the oRNA and sRNA hairpins, indicating that ribose sugar puckers are not significantly influenced by phosphorothioate substitution. The ribose of A_{-10} adopts a conformation intermediate between C2′-*endo* and C3′-*endo* while the ribose groups of the flanking base pairs adopt the C3′-*endo* conformation. Strong P−H5′ and P−H5″ cross-peaks in ^{31}P-^{1}H HetCor spectra indicate non-trans conformations about β at P_{-10} in both the oRNA and sRNA molecules, but lack of stereospecific H5′/H5″ assignments prevented the identification of constraints for this torsion angle. Couplings between C_{-11} C2′ and P_{-11} are <5.0 Hz in both molecules, indicating trans conformations for the C_{-11} ϵ torsion angles. In the sRNA molecule, however, the coupling between C_{-11} C4′ and P_{-11} is also <5.0 Hz, inconsistent with a single ϵ conformation at this residue (*22*). This torsion angle was left unconstrained in the structure calculations.

Models of the oRNA and sRNA hairpins, calculated using experimentally derived distance and torsion angle constraints, confirm that the bulge region adopts substantially different conformations in the two molecules. Figures 5 and 6 show superpositions of the bulge regions from the converged oRNA and sRNA structures. The conformations of the bulged adenine and the two flanking base pairs are defined in both hairpins by >90 constraints, primarily NOE-derived distances (Table 1). The precision of the bulge region is the same for both sets of structures (0.71 Å RMSD), and the variabilities of the bulged nucleotides' positions also are about the same. The somewhat poor superposition of the C_{-9}·G_{-2} base pair flanking the 3′ side of the bulged nucleotide and the A_{-13}·U_{+2} base pair results from bends along the helix axes between the upper and lower stems. However, it should not be concluded that the presence of the bulged A_{-10} nucleotide directly leads to this bending since NMR methods define the long-range structure (such as bending) of helical RNAs less precisely than they define local structure (*22*). Figure 7 compares the bulge regions of the two molecules. In the oRNA hairpin, the base of A_{-10} intercalates between its flanking C_{-11}·G_{-1} and C_{-9}·G_{-2} base pairs, stacking into the RNA helix directly between the pyrimidine rings of C_{-11} and C_{-9}. In the sRNA molecule, the A_{-10} base occupies the major groove, and its flanking base pairs stack against each other.

Since the experimental data indicate that the A_{-10} nucleotide in both molecules has a sugar conformation intermediate between C2′-*endo* and C3′-*endo*, the initial structure calculations were performed with constraints allowing both conformations. These calculations, however, produced oRNA and sRNA structures with exclusively C3′-*endo* and C2′-*endo* A_{-10} conformations, respectively. To test the robustness of the A_{-10} base position with respect to sugar conformation, the A_{-10} sugar of each hairpin was explicitly constrained to C2′-*endo* or C3′-*endo* in separate calculations. In the oRNA hairpin, A_{-10} C2′-*endo* constraints do not alter A_{-10}−C_{-9} stacking, but the A_{-10} base tends to shift toward the *minor* groove side of the helix, partially destacking from the C_{-11} base. In the sRNA hairpin, A_{-10} C3′-*endo* constraints only slightly modify the stacking of the G_{-1}·C_{-11} and G_{-2}·C_{-9} base pairs, but the A_{-10} base shifts from being nearly planar with the G_{-1}·C_{-11} base pair and extends toward the hairpin loop, parallel with the helix axis. This latter conformation predicts several intense yet unobserved NOEs and so does not adequately satisfy the experimental data. In both cases, the calculations produce fewer converged structures. Thus,

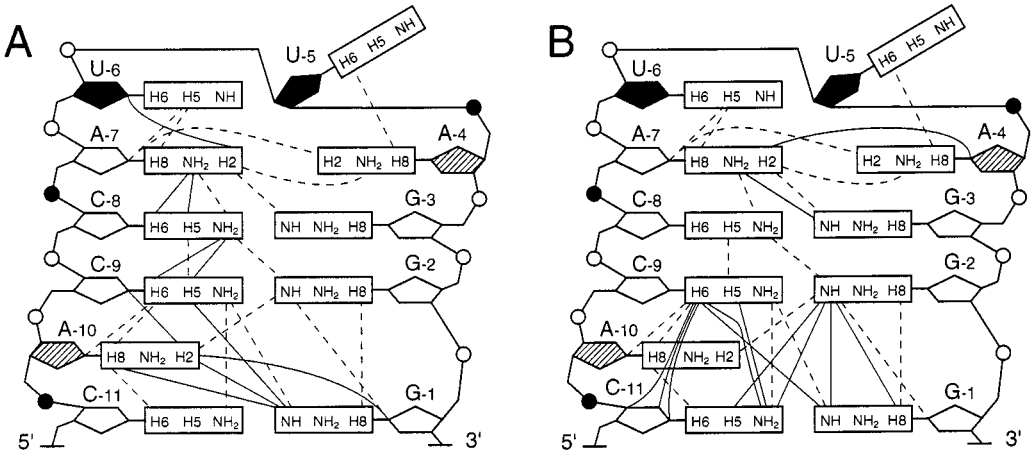

FIGURE 4: Schematic diagram summarizing several key NOEs identified in the bulge and loop regions of the (A) oRNA and (B) sRNA hairpins. Solid lines indicate NOEs identified in only one of the hairpins. Dashed lines indicate NOEs identified in both hairpins. Ribose sugar conformations are indicated as C3′-*endo* (open), C2′-*endo* (filled), or mixed C3′/C2′-*endo* (hatched).

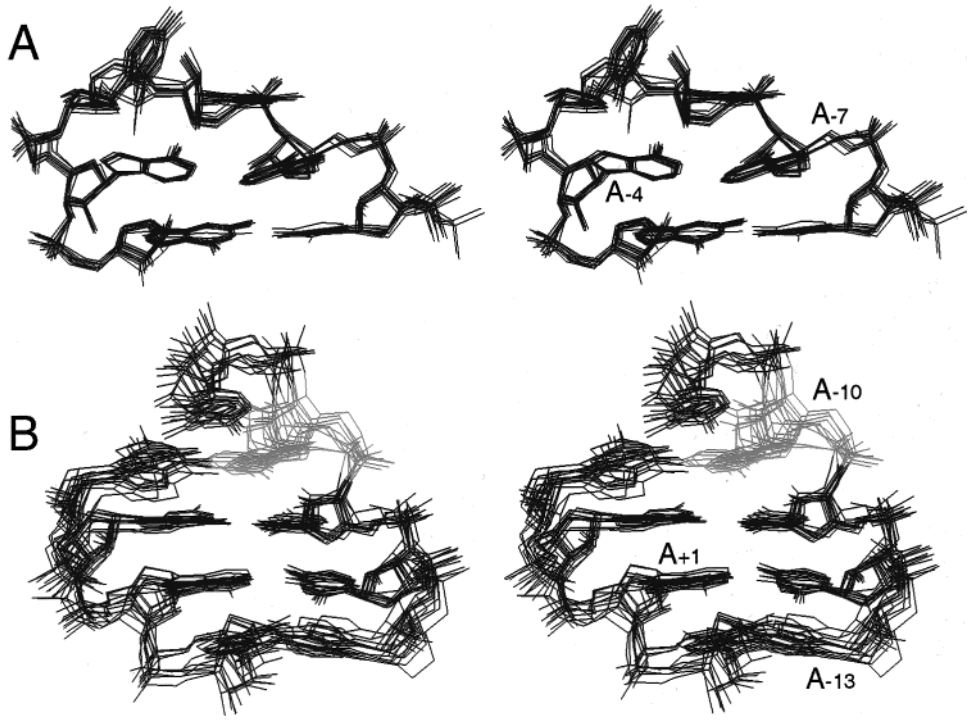

FIGURE 5: Stereo superposition of (A) the loop region (C_9−G_{14}) and (B) the bulge region (A_4−C_8 and G_{15}−U_{18}) from the 10 lowest-energy structures of the oRNA hairpin. Structures are from oRNA calculations with A_{-10} C3′-*endo* constraints. Only sugar and base heavy atoms are shown. Heavy atom RMSDs between the overlain structures and the average structure are 0.40 and 0.71 Å for the loop and stem regions, respectively.

the principal structural features of the bulged A_{-10} nucleotide are largely independent of its sugar conformation, but the details of how the A_{-10} base is accommodated within the helix differ.

Effect of Phosphorothioate Substitution on Conformation of the Stem and Loop Regions. Nucleotides in the stem (G_{-16}−U_{-12}, A_{+1}−C_{+5}) and loop (C_{-8}−G_{-3}) appear to accommodate phosphorothioate substitution without substantial change in conformation. In both the oRNA and sRNA hairpins, sequential base to H1′ NOEs are continuous at τ_m = 180 ms, but interresidue U_{-6}−U_{-5} and U_{-5}−A_{-4} correlations are weak, consistent with C2′-*endo* conformations for U_{-6} and U_{-5}. Also in both molecules, a sequential A_{-4} H2 to G_{-3} H1′ NOE suggests stacking of the A_{-4} and G_{-3} bases. It is worth noting that an analogous NOE is not observed for a similar hairpin in which the closing base pair of the AUUA loop is G_{-8}·C_{-3}, and on which the A_{-4} base does not stack (*32*).

Few differences in the sugar−phosphate backbone of the stem and loop regions could be detected from the available NMR data. As in the bulge region, ribose conformations are similar for both molecules. U_{-6} and U_{-5} adopt the C2′-*endo* conformation, A_{-4} adopts a conformation intermediate between C2′-*endo* and C3′-*endo*, and all other residues adopt the C3′-*endo* conformation. For both molecules, HetCor spectra indicate non-trans conformations about β at P_{-4}. Interestingly, a correlation between P_{-4} and U_{-5} H2′ is present in the HetCor spectrum of the oRNA hairpin but is absent from that of the sRNA hairpin. This difference suggests that the P_{-4} ϵ,ζ torsion angle pair adopts a more

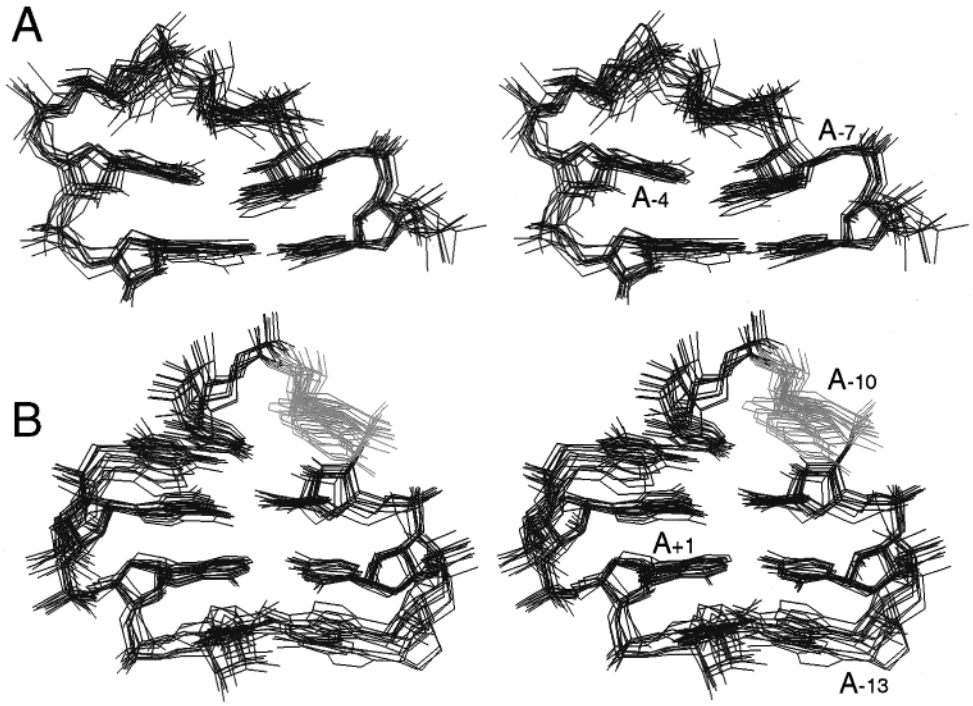

FIGURE 6: Stereo superposition of (A) the loop region and (B) the bulge region from the 10 lowest-energy structures of the sRNA hairpins. Structures are from sRNA calculations with A_{-10} C2′-*endo* constraints. Only sugar and base heavy atoms are shown. Heavy atom RMSDs between the overlain structures and the average structure are 0.71 and 0.72 Å for the loop and stem regions, respectively.

planar 'W' conformation (g^-,t) in the oRNA hairpin than in the sRNA hairpin. The different chemical shifts of the P_{-6} resonances indicate that the backbone conformation between U_{-6} and A_{-7} may be altered by the neighboring phosphorothioate substitution. The ≈0.4 ppm downfield shift of the P_{-6} resonance in the sRNA hairpin suggests that α or ζ at this site tends to have more trans character (*33*), possibly allowing the U_{-6}, A_{-7}, and C_{-8} bases to stack as they do in the oRNA hairpin. Finally, at several stem positions, P−H4′ correlations suggest a t,g^+ conformation for the β,γ dihedral angle pair for both molecules (*22*).

Figures 5 and 6 show the superpositions of the loops. Unlike the bulge regions, the precision to which the loops of the two hairpins are defined differ significantly—0.40 and 0.71 Å RMSD for oRNA and sRNA, respectively. The precision of the oRNA hairpin loop is similar to that achieved for another RNA hairpin containing the AUUA nucleotide sequence (*32*). The oRNA hairpin has ≈4 more distance constraints per loop residue than the sRNA, and several of these constraints involve protons of nucleotides A_{-7} and A_{-4}. The lack of isotopic enrichment of the adenine nucleotides in the sRNA molecule and the terminal positions of A_{-7} and A_{-4} in the loop presumably lead to the lower precision of the sRNA loop.

Figure 7 compares the loop regions from calculated structures of the oRNA and sRNA hairpins. In both molecules, the base of A_{-7} extends across the major groove and stacks on the C_{-8}•G_{-3} base pair. The base of U_{-6} stacks on that of A_{-7}, and the base of U_{-5} extends into the major groove away from the loop. Interestingly, the phosphorothioate at P_{-7} does not impair stacking of A_{-7}. In many of the converged structures, the base of A_{-4} is roughly coplanar with the base of A_{-7}, but there is no experimental evidence for hydrogen bonds between the two bases (*32*). In the oRNA hairpin, the helical twist between A_{-4} and G_{-3} is discontinuous, the A_{-4} base is recessed into the minor groove, and the A_{-4} 2′-OH points into the major groove. In the sRNA hairpin, the A-form helix of the upper stem continues into the loop, allowing the A_{-4} base to stack on G_{-3} with the A_{-4} 2′-OH pointing into the minor groove. Although the torsion angles of the phosphate backbone within each family of calculated structures are somewhat variable, the phosphate and the phosphorothioate families have different configurations of α, β, and ζ at P_{-4}. In the oRNA hairpin, these angles often adopt the g^-/t,t/g^-,g^+ conformations, but in the sRNA hairpin, these angles are more often g^-,g^-,t. The geometry of the lower stem in both molecules is very similar to that of a standard A-form helix. The α and ζ torsion angles at P_{-13} and P_{+1} were left unconstrained in all calculations and usually adopt the A-form g^-,g^- conformation in both hairpins.

Effect of Phosphorothioate Substitution on RNA Stability. The thermal stability of the two hairpins was investigated using UV melting experiments to measure overall molecular stability (T_m) and using the temperature dependence of base ^{1}H chemical shifts to assess the stability of specific nucleotides (T_{cs}). The UV melting experiments yield T_m values of 60 and 65 °C for the oRNA and sRNA hairpins, respectively (Figure 8). The increased stability of the sRNA hairpin is unexpected, since R_P phosphorothioate substitution in oligonucleotide DNA duplexes destabilizes the duplex and *decreases* T_m (*30*, *34*).

In an effort to identify specific regions of the hairpin that might be preferentially stabilized by phosphorothioate substitution, the temperature dependencies of adenine H2 and pyrimidine H5 base chemical shifts were determined for both hairpins. These chemical shifts are sensitive to the degree of base stacking within the helix, but quantitative interpretation of the shifts can be complicated by chemical exchange processes (*35*). In the oRNA hairpin, nucleotides near the 3′

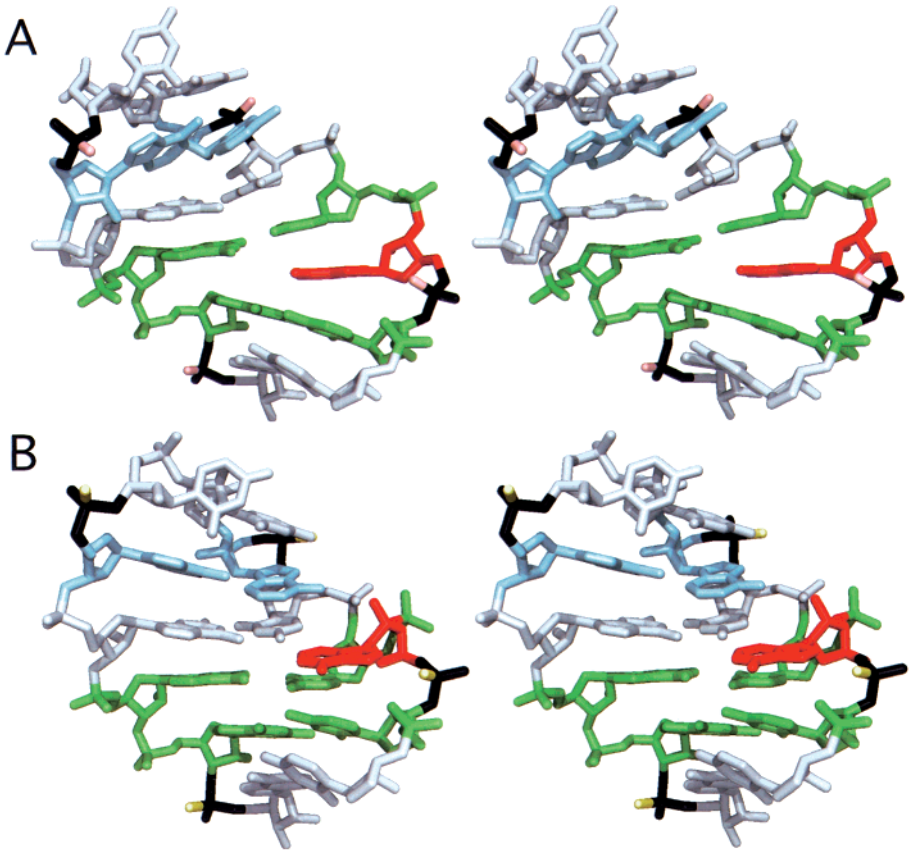

FIGURE 7: (A, B) Stereoview of the bulge and loop regions from minimized average structures of the (A) oRNA and (B) sRNA hairpins. View is into the major groove. A_{-10} is shown in red, C_{-11}·G_{-1} and C_{-9}·G_{-2} base pairs are shown in green, and A_{-7} and A_{-4} are shown in blue. Positions of phosphorothioate substitution are shown in black, R_P oxygen atoms are shown in pink, and R_P sulfur atoms are shown in yellow. Phosphorothioate substitution causes little or no change in the conformation of the stem and loop regions but extrudes A_{-10} out of the RNA helix into the major groove. This rearrangement dramatically alters the array of functional groups accessible at the surface of the molecule.

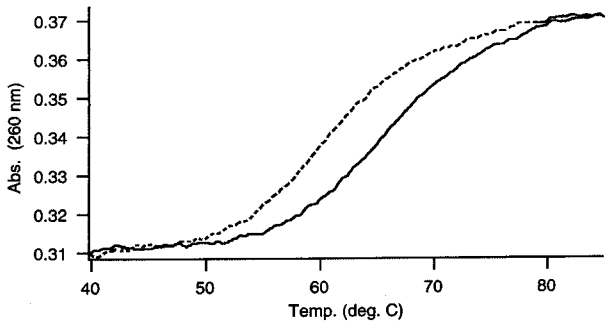

FIGURE 8: Overlay of the UV melting curves of the oRNA (dashed line) and sRNA (solid line) hairpins. The T_m's of the oRNA and sRNA hairpins are 60 and 65 °C, respectively. The uncertainty in each value is ±0.5 °C.

end of the loop have the lowest transition midpoints (T_{cs}), indicating that this region is the least stable. The most stable region is the center part of the lower stem. The sRNA hairpin exhibits the same trend, but phosphorothioate groups in the loop and stem slightly enhance the stability of adjacent nucleotides, leading to T_{cs} values 3−5 °C higher than those observed for the oRNA hairpin (Table 2).

The temperature dependencies of the oRNA and sRNA A_{-10} H2 resonances differ but are consistent with the NMR-derived conformations of the A_{-10} bases. The chemical shift of the oRNA A_{-10} H2 shifts downfield 0.21 ppm and has a T_{cs} of 59 °C, but the sRNA A_{-10} H2 resonance does not exhibit a temperature-dependent chemical shift change. In the sRNA, the bulged adenine base is extrahelical, and its H2 resonance is not expected to be influenced significantly by ring currents of the flanking bases. However, since the bulged adenine base of the oRNA hairpin stacks into the helix, the chemical shift of its H2 resonance is expected to change as the helix melts. Another difference between the two molecules is that the H8 of G_{-2} and G_{-1} in the sRNA hairpin each give rise to a pair of resonances differing by ≈0.15 ppm at ∼57 °C. This doubling of resonances is not observed in the oRNA hairpin. Resonance doubling on the partner strand could not be detected for either molecule, although crowding could partially obscure doubling of the C_{-11} and C_{-9} H6 and H5 resonances. The doubling of peaks occurs near the T_{cs} of G_{-2} and G_{-1} and is likely the result of slow exchange of the phosphate backbone between two conformations or partial local destacking around the bulge just prior to melting.

DISCUSSION

We have found that phosphorothioate substitution substantially alters the conformation of an RNA hairpin containing the binding site for phage MS2 capsid protein. This hairpin contains a single bulged adenine necessary for protein binding that, in the unmodified form of the free RNA, stacks into the helix between its flanking base pairs (Figure 7A). When the phosphates 5′ to all five adenine residues in this hairpin are replaced with R_P phosphorothioates, the bulged

Table 2: T_{cs} Values for Resolved Adenine H2 and Pyrimidine H5 Resonances of the oRNA and sRNA Hairpins[a]

	A_{-13}	U_{-12}	C_{-11}	A_{-10}	C_{-9}	C_{-8}	A_{-7}	U_{-6}	U_{-5}	A_{-4}	A_{+1}	U_{+2}	C_{+3}	U_{+4}	C_{+5}
oRNA	58	64	60	59	−	58	61	62	nc	nc	58	59	−	60	54
sRNA	−	65	65	nc	−	64	−	63	nc	nc	−	64	−	63	61

[a] (−) indicates that the resonance could not be identified unambiguously at elevated temperatures, and nc indicates that the chemical shift of the resonance does not change with temperature. All resonances had chemical shift changes ≥0.2 ppm downfield, and all T_{cs} values are ±2.0 °C.

adenine is extruded into the major groove, and its flanking base pairs stack against each other to close the gap (Figure 7B). This conformational rearrangement dramatically alters the array of functional groups and electrostatic charges accessible at the surface of the molecule. For example, the major groove face of the cytidine 3′ to the extruded adenine is buried entirely and shielded from potential interactions with proteins or other ligands. While the MS2 capsid protein makes no known contacts to this cytidine, the ability of phosphorothioates to alter RNA conformation suggests that the phosphorothioate substitution−interference experiments commonly used to identify phosphate sites involved in RNA−ligand binding may be vulnerable to conformational artifacts.

Despite the large effect at the bulged adenine, most modified sites accommodate phosphorothioate substitution with little or no change in conformation. Substitution increases the stability of adjacent A-form nucleotides and increases the stacking between A_{-4} and G_{-3} but does not seem to affect ribose sugar puckers or the stacking of A_{-7}. The minor effects seen are similar in magnitude to those observed for substitutions in helical regions of DNA, which cause adjacent deoxyribose sugars to populate the C3′-*endo* conformation to a greater extent but leave the overall structure largely unchanged (*11*). These results suggest that changes in conformation caused by phosphorothioate substitution are likely to be restricted to regions of nucleic acids with irregular secondary structure.

Possible Mechanisms of Phosphorothioate-Induced Conformational Change. We envision at least two possible ways in which substitution could alter RNA conformation. First, the large size of the sulfur atom may prevent the phosphate backbone around P_{-10} from adopting a geometry required for the bulged adenine to stack into the helix. For example, steric hindrance between the R_P sulfur atom and the adjacent C3′ or C5′ atoms may prevent certain configurations of the α and ζ torsion angles. These torsion angles cannot be measured directly using NMR spectroscopy, but α and ζ conformations have been empirically correlated in DNA with the chemical shift of the intervening ^{31}P nucleus (*33*). Similar chemical shift correlations have not been derived for RNA or for phosphorothioate-modified nucleic acids, but the reversed resonance positions of P_{-10} relative to P_{-13}, P_{-7}, and P_{+1} in the oRNA and sRNA molecules suggest that the hairpins may have different α and ζ geometries. Indeed, these angles tend to have different conformations in the calculated structures of the two hairpins. This is consistent with quantum mechanical free energy calculations which predict different α and ζ torsion angle conformations for phosphates and phosphorothioates (*36*). It is also noteworthy that the backbone around P_{-10} tends to have a more regular A-form geometry in structures of the phosphorothioate-modified hairpin than those of the unmodified hairpin. It is possible that R_P phosphorothioate substitution destabilizes non-A-form backbone geometries. If so, this would also account for our observation that modification provides greater thermal stability to adjacent A-form RNA nucleotides.

Alternatively, phosphorothioate substitution could alter RNA conformation indirectly by modifying the hydration pattern of the hairpin. RNA helices contain a network of water molecules in the major groove connecting adjacent phosphates through their *pro*-R_P phosphoryl oxygen atoms (*37*). Although phosphorothioate substitution does not change the net charge of the phosphate backbone, the different size and polarizability of the sulfur atom may alter the organization of bound water molecules in the major groove and destabilize the stacked conformation of the unpaired adenine. Organized water molecules have been shown to play an important role in stabilizing the complex between homeodomain protein MATα2 and its DNA recognition duplex (*38*). Methylphosphonate substitution interferes with formation of the protein−DNA complex at discrete stereospecific phosphoryl oxygen sites, some of which contact the homeodomain protein only indirectly through bound water molecules. Although phosphorothioate substitution at these sites does not affect the hydration network of the MATα2−DNA complex, the cumulative effect of multiple substitutions in a single molecule, such as in our study, may be sufficient to affect the bound water structure of RNA.

Implications for Binding of Phage MS2 Capsid Protein to Its RNA Operator. In light of the large effect phosphorothioate substitution has on the conformation of the bulged adenine, it is unusual that substitution at this site has no effect on binding of the hairpin to phage MS2 capsid protein (*7*). The bulged adenine plays a crucial role in formation of the protein−RNA complex and is essential for protein binding (*39*). In crystal structures of the complex, the bulged adenine is looped out of the helix into the major groove and makes several specific contacts in a pocket on the surface of the protein (*40*). While there are no contacts to P_{-10}, it is reasonable to expect a conformational change of the sort observed in our study to increase binding affinity by reducing the amount of structural rearrangement within the hairpin stem necessary to form the protein−RNA complex. The lack of an observed effect might be due to sequence differences between the RNA hairpin used in our study and those used in substitution−interference experiments. The bulged adenine in our hairpin is flanked by cytidine residues, while in most hairpins used for phosphorothioate interference experiments the bulged adenine is flanked by guanine nucleotides (*7*). It is possible that the large conformational change we observe is sensitive to this molecular context and would not occur for different flanking base pairs. Alternatively, phosphorothioate substitution at P_{-10} could fail to alter binding affinity because conformational rearrangement of the hairpin loop, rather than the bulged adenine, is the rate-limiting step in formation of the protein−RNA complex. This is supported by the observation that a variant hairpin containing an

unusual A-(A•U) bulge motif with a hydrogen bond to a protonated adenine has a binding affinity that is unaffected by pH (*32*), and by the observation that the variant AUCA tetraloop binds nearly 100-fold more tightly than the wild-type AUUA due to an intramolecular hydrogen bond that stabilizes the protein-bound loop conformation (*40*).

Of the five phosphorothioate substitutions in the sRNA hairpin, only one has a measurable effect on binding affinity (*7*). Substitution of P_{-7} with R_P phosphorothioate increases binding affinity 4-fold (*7*). Since the structure of this site in the sRNA hairpin is virtually identical to that in the oRNA hairpin and to that in the protein−RNA complex (*40*), our data support earlier interpretations (*41*) that the increase in affinity is due to reinforcement of an electrostatic interaction between the R_P phosphoryl sulfur atom and Lys57 of the capsid protein. Substitution of P_{-6} with R_P phosphorothioate or with phosphorodithioate increases binding affinity 20-fold (*41*) despite the fact that there are no contacts between P_{-6} and the capsid protein in crystal structures of the complex (*40*). In light of the results presented here, we propose that the R_P sulfur atom destabilizes the conformation of the free RNA, in which the base of U_{-6} stacks on the base of A_{-7} with a non-A-form backbone geometry around P_{-6}, and thus increases binding affinity by promoting faster rearrangement between the free and bound conformations of the hairpin loop.

CONCLUSIONS

Phosphorothioate substitution−interference experiments are a useful and widespread way to identify specific phosphoryl oxygen sites in nucleic acids that form direct contacts with ligands such as proteins or divalent metal ions and sites that participate in RNA-directed catalysis. We have found, however, that phosphorothioate substitution can have large effects on the conformation of RNA molecules. These results suggest that phosphoryl oxygen sites identified by substitution−interference experiments have the potential to be false positives that are not directly involved with the biological function of the RNA being studied. Instead, substitution at these sites may alter the conformation of the molecule from its biologically active state. Phosphorothioate substitution appears to be less likely to alter conformation in regions of regular duplex secondary structure, but the fact that many of the functionally important regions of RNA molecules have irregular or unusual secondary structures complicates the use of substitution−interference experiments to study RNA structure and function.

ACKNOWLEDGMENT

We thank Dr. K. Kalurachchi and K. McKinney for assistance with spectral analysis and for helpful discussions. We also thank Dr. S. Moran for assistance with acquisition and analysis of the UV melting curves and Dr. D. Gorenstein for providing access to the Varian 600 MHz NMR spectrometer at UTMB.

SUPPORTING INFORMATION AVAILABLE

Four tables containing the ^{1}H, ^{13}C, ^{15}N, and ^{31}P resonance assignments and Figure S1 containing the HetCor spectra of the oRNA and sRNA hairpins (6 pages). This material is available free of charge via the Internet at http://pubs.acs.org.

REFERENCES

1. Heidenreich, O., Pieken, W., and Eckstein, F. (1993) *FASEB J. 7*, 90−96.
2. Ruffner, D. E., and Uhlenbeck, O. C. (1990) *Nucleic Acids Res. 18*, 6025−6029.
3. Chanfreau, G., and Jacquier, A. (1994) *Science 266*, 1383−1387.
4. Jeoung, Y.-H., Kumar, P. K. R., Suh, Y.-A., Taira, K., and Nishikawa, S. (1994) *Nucleic Acids Res. 22*, 3722−3727.
5. Michels, W. J., Jr., and Pyle, A. M. (1995) *Biochemistry 34*, 2965−2977.
6. Kufel, J., and Kirsebom, L. A. (1998) *RNA 4*, 777−788.
7. Milligan, J. F., and Uhlenbeck, O. C. (1989) *Biochemistry 28*, 2849−2855.
8. Schnitzer, W., and von Ahsen, U. (1997) *Proc. Natl. Acad. Sci. U.S.A. 94*, 12823−12828.
9. Cruse, W. B. T., Salisbury, S. A., Brown, T., Cosstick, R., Eckstein, F., and Kennard, O. (1986) *J. Mol. Biol. 192*, 891−905.
10. Bachelin, M., Hessler, G., Kurz, G., Hacia, J., Dervan, P., and Kessler, H. (1998) *Nat. Struct. Biol. 5*, 271−276.
11. Gonzalez, C., Stec, W., Kobylanska, A., Hogrefe, R. I., Reynolds, M., and James, T. L. (1994) *Biochemistry 33*, 11062−11072.
12. Davanloo, P., Rosenburg, A. H., Dunn, J. J., and Studier, F. W. (1984) *Proc. Natl. Acad. Sci. U.S.A. 81*, 2035−2039.
13. Milligan, J. F., Groebe, D. R., Witherell, G. W., and Uhlenbeck, O. C. (1987) *Nucleic Acids Res. 15*, 8783−8789.
14. Nikonowicz, E. P., Sirr, A., Legault, P., Jucker, F. M., Baer, L. M., and Pardi, A. (1992) *Nucleic Acids Res. 20*, 4507−4513.
15. Cohn, W. E. (1950) *J. Am. Chem. Soc. 72*, 1471−1478.
16. Eckstein, F., and Goody, R. S. (1976) *Biochemistry 8*, 1685−1691.
17. Pardi, A., and Nikonowicz, E. P. (1992) *J. Am. Chem. Soc. 114*, 9202−9203.
18. Legault, P., Farmer, B. T., II, Mueller, L., and Pardi, A. (1994) *J. Am. Chem. Soc. 116*, 2203−2204.
19. Sklenar, V., Peterson, R. D., Rejante, M. R., and Feigon, J. (1994) *J. Biomol. NMR 4*, 117−122.
20. Williamson, D., and Bax, A. (1988) *J. Magn. Reson. 76*, 174−177.
21. Legault, P., Jucker, F. M., and Pardi, A. (1995) *FEBS Lett. 362*, 156−160.
22. Varani, G., Aboul-ela, F., and Allain, F. H.-T. (1996) *Prog. Nucl. Magn. Reson. Spectrosc. 29*, 51−127.
23. Santos, R. A., Tang, P., and Harbison, G. S. (1989) *Biochemistry 28*, 9372−9378.
24. Altona, C. (1982) *Recueil Rev. 101*, 413−433.
25. Brünger, A. T. (1992) *X-PLOR Version 3.1 Manual*, Yale University, New Haven, CT.
26. Jaroszewski, J. W., Syi, J.-L., Maizel, J., and Cohen, J. S. (1992) *Anti-Cancer Drug Des. 7*, 253−262.
27. Pardi, A. (1995) *Methods Enzymol. 261*, 350−380.
28. Dieckmann, T., and Feigon, J. (1997) *J. Biomol. NMR 9*, 259−272.
29. Otting, G., and Wuthrich, K. (1990) *Q. Rev. Biophys. 23*, 39−96.
30. LaPlanche, L. A., James, T. L., Powell, C., Wilson, W. D., Uznanski, B., Stec, W. J., Summers, M. F., and Zon, G. (1986) *Nucleic Acids Res. 14*, 9081−9093.
31. Furrer, P., Billeci, T. M., Donati, A., Kojima, C., Karwowski, B., Sierzchala, A., Stec, W., and James, T. L. (1999) *J. Mol. Biol. 285*, 1609−1622.
32. Smith, J. S., and Nikonowicz, E. P. (1998) *Biochemistry 37*, 13486−13498.
33. Gorenstein, D. G. (1984) *Phosphorus-31 NMR: Principles and Applications*, Academic Press, New York.
34. Jaroszewski, J. W., Clausen, V., Cohen, J. S., and Dahl, O. (1996) *Nucleic Acids Res. 24*, 829−834.
35. Pardi, A., Martin, F. H., and Tinoco, I. J. (1981) *Biochemistry 20*, 3986−3996.

36. Florian, J., Strajbl, M., and Warshel, A. (1998) *J. Am. Chem. Soc. 120*, 7959−7966.
37. Egli, M., Portmann, S., and Usman, N. (1996) *Biochemistry 35*, 8489−8494.
38. Labeots, L. A., and Weiss, M. A. (1997) *J. Mol. Biol. 269*, 113−128.
39. Carey, J., and Uhlenbeck, O. C. (1983) *Biochemistry 22*, 2610−2615.
40. Valegård, K., Murray, J. B., Stonehouse, N. J., van den Worm, S., Stockley, P. G., and Liljas, L. (1997) *J. Mol. Biol. 270*, 724−738.
41. Johansson, H., Dertinger, D., LeCuyer, K. A., Behlen, L. S., Greef, C. H., and Uhlenbeck, O. C. (1998) *Proc. Natl. Acad. Sci. U.S.A. 95*, 9244−9249.

BI992712B